Traces of stable and unstable manifolds in heat flux patterns

A. Wingen, M. Jakubowski, K. H. Spatschek, S. S. Abdullaev, K. H. Finken, M. Lehnen, and TEXTOR team

Citation: Physics of Plasmas **14**, 042502 (2007); doi: 10.1063/1.2715548
View online: https://doi.org/10.1063/1.2715548
View Table of Contents: http://aip.scitation.org/toc/php/14/4
Published by the American Institute of Physics

Traces of stable and unstable manifolds in heat flux patterns

A. Wingen
Institut für Theoretische Physik, Heinrich-Heine-Universität Düsseldorf, D-40225 Düsseldorf, Germany

M. Jakubowski
Institut für Plasmaphysik, Forschungszentrum Jülich GmbH, EURATOM Association, Trilateral Euregio Cluster, D-52425 Jülich, Germany

K. H. Spatschek
Institut für Theoretische Physik, Heinrich-Heine-Universität Düsseldorf, D-40225 Düsseldorf, Germany

S. S. Abdullaev, K. H. Finken, and M. Lehnen
Institut für Plasmaphysik, Forschungszentrum Jülich GmbH, EURATOM Association, Trilateral Euregio Cluster, D-52425 Jülich, Germany

TEXTOR team

(Received 15 January 2007; accepted 20 February 2007; published online 12 April 2007)

Experimental observations of heat fluxes on divertor plates of tokamaks show typical structures (boomerang wings) for varying edge safety factors. The heat flux patterns follow from general principles of nonlinear dynamics. The pattern selection is due to the unstable and stable manifolds of the hyperbolic fixed points of the last intact island chain. Based on the manifold analysis, the experimental observations can be explained in full detail. Quantitative results are presented in terms of the penetration depths of field lines. © *2007 American Institute of Physics*.
[DOI: 10.1063/1.2715548]

I. INTRODUCTION

Nonlinear signatures of particle and heat transport are generic in fluid dynamics, soft matter, and plasma physics, astrophysics, etc.[1] Transport anomalies reach from Bohm-like diffusion in gas discharges up to low-energy cosmic ray penetration into the heliosphere.[2,3] Anomalous particle and heat losses have enormous consequences for practical applications. For example, in magnetic fusion devices, heat fluxes should be relatively low and well distributed over the wall to reach tolerable local power depositions; see, e.g., Ref. 4 and references therein. Therefore, it is desirable to identify the basic processes which rule anomalous losses from open nonlinear (chaotic) systems. The main purpose of the present paper is to formulate, prove, and quantify selection rules for spatial heat flow patterns at the boundaries of stochastic plasmas. In order to analyze and classify the spatial structures of heat flux patterns, we propose the concept of magnetic footprints[5,6] together with an analysis of the stable and unstable manifolds of hyperbolic periodic points[7–10] of the last intact island chain. The latter is the last resonance in front of the wall at the transition from the ergodic zone to the laminar zone.[11]

The magnetic field line dynamics is one aspect.[12] As it is well known, magnetic field lines represent a $1+1/2$ degree-of-freedom Hamiltonian system. This fact is important for the description of field lines by flux-preserving mappings, which are computationally efficient and powerful tools to study field lines in the presence of nonaxisymmetric magnetic perturbations. Numerous mapping models of field lines in a toroidal system have been proposed to study the destruction of nested magnetic surfaces and the formation of stochastic magnetic field lines (see Refs. 11 and 13–19 and references therein). The main goal of mapping models is to replace the original continuous dynamical system, the magnetic field lines, by a discrete iterative map, which runs much faster then the small-step numerical integration.[15,18–21] Mappings should be symplectic (or flux preserving). They should have the same periodic points as the Poincaré map of the original system, and they should show the same regular and chaotic regions as the continuous magnetic field line evaluation. For global maps, a magnetic axis should be mapped to itself, and the magnetic flux should be always positive.[13] Thus, the transition to useful discrete maps is by no means trivial.

Another aspect of transport is the dynamics of particles in a magnetic field. It is known that in inhomogeneous magnetic fields particle orbits deviate from the magnetic field lines.[22] An important question is how this can affect the transport of particles in a stochastic magnetic field. The enhanced transport of heat and particles due to destroyed nested magnetic surfaces has been analyzed in the past in a number of publications (see Refs. 23–30).

In a plasma of typically $kT=10$–20 keV temperature, most of the particles move with the thermal velocity. According to recent studies of particle drift effects,[31,32] only particles with kinetic energies much larger than the thermal one show relevant drift effects. Thermal particles can be considered to follow very well the field lines as long as binary collisions are weak. In the present paper we model the heat flux characteristics in collisionless plasmas by the transport along the stochastic magnetic field lines. It turns out that experimentally observed heat flux patterns are the traces of stable and unstable manifolds of the last intact island chain.

The paper is organized as follows. In Sec. II we present

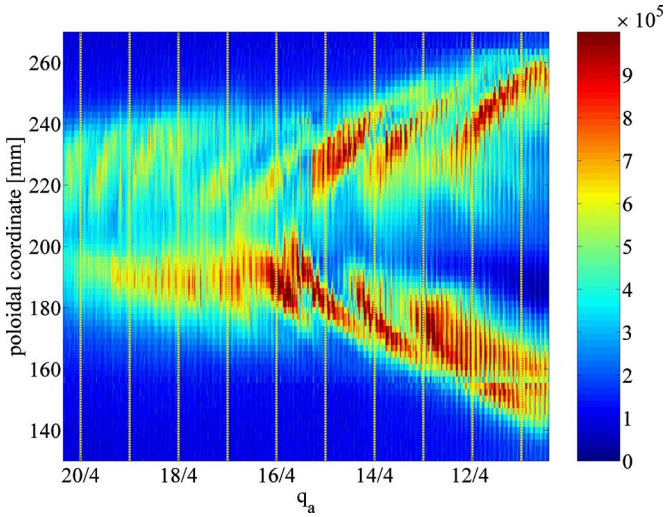

FIG. 1. (Color online) Measurement of the heat flux pattern with changing edge safety factor q_a at a fixed toroidal position of the divertor plates. The red colors (dark wings) indicate hot areas.

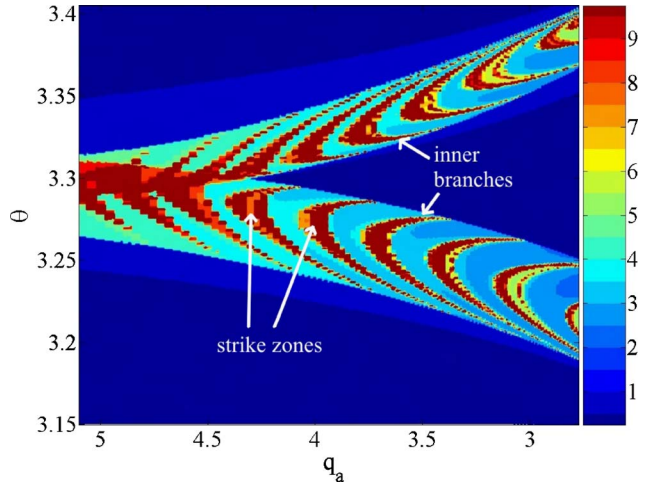

FIG. 2. (Color online) Calculations of connection lengths at a fixed toroidal position dependent on the poloidal angle θ and (decreasing) edge safety factor q_a for one stripe. The colors indicate the connection lengths in toroidal turns (dark wings in black and white correspond to large connection lengths).

new results on measured heat flux patterns as well as the interpretation due to large connection lengths. Poincaré plots of the magnetic field are shown in Sec. III. There we also determine hyperbolic fixed points. The stable and unstable manifolds of the latter are very important for the understanding of the observed heat flux patterns. In Sec. IV we investigate how hot particles follow the manifolds and move toward the wall. We discuss the relation to the so-called MASTOC (magnetic stochastic configuration) criterion.[33] The magnetic field model is defined in the Appendix. The paper is concluded by a short summary.

II. PHENOMENOLOGY OF HEAT FLUX PATTERNS

Edge stochastization is a candidate for the plasma-wall-interaction control.[34–37] Characteristic spatial heat flux patterns have been observed in the tokamaks Tore Supra[33] and DIII-D.[34] Our recent measurements[38,39] in TEXTOR with a dynamic ergodic divertor (DED)[11] also show typical structures with a characteristic number of stripes on the target plates, when visualized in the (φ,θ) plane. Here φ is the toroidal angle and θ is the poloidal angle of the torus. The DED is operated in the so-called $12/4 \equiv m/n$ base mode. The latter specifies the current configuration in the DED perturbation coils. The ratio $m/n \equiv q$ corresponds to the ratio of n poloidal and m toroidal turns of a closed (unperturbed) field line. Four heat flux stripes were observed at the divertor plates.[39] The number of stripes is related to the toroidal main mode number $n=4$. Figure 1 shows a typical heat flux stripe dependent on the edge safety factor q_a. The picture is taken at a fixed toroidal position over the small poloidal angle area covered by one heat flux stripe. Each stripe consists of an upper and lower part. When varying the edge safety factor q_a, and projecting on the (q_a,θ) plane, boomerang-like structures appear. The edge safety factor is inversely proportional to the plasma current; the latter has been varied. All other parameters are kept constant. At certain values of q_a new strike zones appear, while the former strike zone tends outwards (compared to the center of the figure), gets smaller, and finally vanishes. The strike zones overlap.

Plasma structures are strongly influenced by the stochastic magnetic field topology.[40] Thermal particles mainly follow the field line dynamics.[31] We use the field line mapping technique in its symmetrical form[19] to determine the magnetic field topology and thereby the plasma structure. It is suggestive to relate the heat flux patterns to areas of long connection lengths of magnetic field lines, assuming that the latter can penetrate deep into the hot plasma area. At the plasma edge, a stochastic magnetic field line enters the system and goes along the torus, before leaving the system. The length of a field line within the system is the connection length of the field line. The connection lengths can be visualized in a so-called laminar plot. This is a colored contour plot in a poloidal (θ,r) cross section, where the colors indicate the connection lengths of field lines passing through, or hitting, the respective area. For comparing with the heat flux pattern of Fig. 1, we calculated 97 laminar plots for different plasma currents, from $I_p=228$ to 420 kA in 2 kA steps. Collecting the values at the wall radius $r_w=0.477$ m (the minor plasma radius is $a=0.437$ m), we obtained Fig. 2 for the DED perturbation current $I_0=11.4$ kA. For example, more than 10 toroidal iterations are needed for field lines of the red areas in Fig. 2 to get from wall to wall.

In Fig. 2 we can identify zones similar to the experiment. Boomerang-shaped strike zones form two parts diverging with decreasing q_a. However, the inner branches of the boomerang-shaped strike zones are not observed in the measurement. As we shall show, both phenomena, the periodic variations (with decreasing q_a values) of the strike zones and the missing of the inner branches, follow from the fact that the stable and unstable manifolds of the last intact island chain determine the observable heat flow patterns. In other words, not only the lengths of the field lines are important, but also the radial penetration depths.[33] The latter increase for magnetic field lines close to the manifolds; the reason is

the rapid transport along the interactions of manifolds belonging to different island chains.[9]

III. THE ROLE OF HYPERBOLIC FIXED POINTS

In this section we determine the hyperbolic fixed points of the last intact island chain in an ergodic divertor plasma. Details of the equilibrium plasma configuration and the perturbation magnetic field can be found in the Appendix. First, we calculate Poincaré plots of magnetic field lines by using the fast mapping technique. The plots are created by tracing field lines and marking the intersections of the field lines with a preselected poloidal section.

A. Magnetic field lines

It is known that a divergence-free magnetic field is equivalent to a Hamiltonian system with $1+1/2$ degrees of freedom (see, e.g., Refs. 41–43). Particularly, the magnetic field $\mathbf{B}$ can be presented in the Clebsch form $\mathbf{B}=B_0R_0^2(\nabla\psi\times\nabla\vartheta+\nabla\varphi\times\nabla\psi_{\mathrm{pol}})$, where ψ and ψ_{pol} are the toroidal and poloidal fluxes normalized to $B_0R_0^2$, respectively, ϑ is the poloidal (intrinsic) angle θ, and φ is the toroidal angle. Here B_0 is the strength of the toroidal magnetic field at the center of torus R_0. In this coordinate system the field line equations have the Hamiltonian form

$$\frac{d\psi}{d\varphi}=-\frac{\partial H}{\partial\vartheta}\quad\frac{d\vartheta}{d\varphi}=\frac{\partial H}{\partial\psi},\tag{1}$$

where the poloidal flux $H\equiv\psi_{\mathrm{pol}}$ plays the role of a Hamiltonian function, ϑ and ψ are the canonically conjugated coordinate and momentum, respectively, and φ is a time-like independent variable.

In the presence of nonaxisymmetric magnetic perturbations the poloidal flux $H=H(\psi,\vartheta,\varphi)$ can be presented as a sum,

$$H=H_0(\psi)+H_1(\psi,\vartheta,\varphi),\tag{2}$$

where the unperturbed flux $\psi_{\mathrm{pol}}^{(0)}(\psi)$ depends only on the equilibrium magnetic configuration of the plasma. It is determined by the safety factor $q(\psi)$,

$$H_0(\psi)=\int\frac{d\psi}{q(\psi)}.\tag{3}$$

The perturbation flux $\psi_{\mathrm{pol}}^{(1)}(\psi,\vartheta,\varphi)$ can be expanded into a Fourier series in ϑ and φ,

$$H_1(\psi,\vartheta,\varphi)=\epsilon\sum_{m,n}H_{mn}(\psi)\cos(m\vartheta-n\varphi+\chi_{mn}).\tag{4}$$

The Fourier coefficients $H_{mn}(\psi)$ correspond to the poloidal mode number m and the toroidal mode number n. The determination of $H_{mn}(\psi)$ is described in the Appendix.

B. Discrete mapping

In this section we study the stochasticity of field lines created by the external magnetic perturbations at the plasma edge. This will be done by plotting Poincaré sections of magnetic field lines and their stable and unstable manifolds. For this purpose we shall employ the computationally efficient mapping method described in Refs. 19–21. The mapping is constructed in a symplectic (or flux-preserving) form and it is much faster than the other conventional small-step integration schemes, like Runge-Kutta. Below, we shall shortly outline the mapping method. We will use it for finding periodic fixed points and their stable and unstable manifolds.

Let (ϑ_k,ψ_k) be values of the poloidal angle ϑ and the toroidal flux ψ at the poloidal section $\varphi=\varphi_k=k(2\pi/N)$, where $k=0,\pm1,\pm2,\ldots$, and $N\geqslant1$. The relation

$$(\vartheta_{k\pm1},\psi_{k\pm1})=\hat{T}^{(\pm)}(\vartheta_k,\psi_k)\tag{5}$$

defines the mapping of the field line coordinates at the section φ_k to the ones at the section $\varphi_{k\pm1}$. The index $(+)$ corresponds to the mapping along the positive direction of the toroidal angle φ and it is called a *forward map*. Similarly, the index $(-)$ corresponds to a *backward map*, which describes field line dynamics along the negative direction of the toroidal angle.

The mapping (5) is implemented by the successive canonical transformations employing the time-dependent perturbation theory. For the Hamiltonian system (2)–(4) the mapping, in the first order of the perturbation parameter ϵ, has the following form:

$$\Psi_k=\psi_k-\epsilon\frac{\partial S^{(k)}}{\partial\vartheta_k},\quad\Theta_k=\vartheta_k+\epsilon\frac{\partial S^{(k)}}{\partial\Psi_k},$$

$$\bar{\Theta}_k=\Theta_k+\frac{\varphi_{k\pm1}-\varphi_k}{q(\Psi_k)},$$

$$\psi_{k\pm1}=\Psi_k+\epsilon\frac{\partial S^{(k\pm1)}}{\partial\vartheta_{k\pm1}},\quad\vartheta_{k\pm1}=\bar{\Theta}_k-\epsilon\frac{\partial S^{(k\pm1)}}{\partial\Psi_{k\pm1}},\tag{6}$$

where $S^{(k)}\equiv S(\vartheta_k,\Psi_k)$ is the value of the generating function $S(\vartheta,\Psi,\varphi,\varphi_0)$ taken at sections $\varphi=\varphi_k$, i.e., $S(\vartheta_k,\Psi_k)=S(\vartheta_k,\Psi_k,\varphi_k,\varphi_0)$,

$$\begin{aligned}S(\vartheta,\Psi,\varphi,\varphi_0)=&-(\varphi-\varphi_0)\sum_{m,n}H_{mn}(\Psi)\\&\times[a(x_{mn})\sin(m\vartheta-n\varphi+\chi_{mn})\\&+b(x_{mn})\cos(m\vartheta-n\varphi+\chi_{mn})],\end{aligned}\tag{7}$$

defined in the finite interval $\varphi_{k+1}<\varphi<\varphi_k$. Here,

$$a(x)=\frac{1-\cos x}{x},\quad b(x)=\frac{\sin x}{x},$$

$$x_{mn}=\left(\frac{m}{q(\Psi)}-n\right)(\varphi-\varphi_0).$$

The free parameter φ_0 lies in the interval $\varphi_k\leqslant\varphi_0\leqslant\varphi_{k+1}$.

The Poincaré section corresponding to the preselected poloidal section φ_P is obtained by applying the map (5) N times, when field lines return to the poloidal section φ_P.

The map (6) provides us with the Poincaré plot for the magnetic field lines of the TEXTOR-DED configuration. Figure 3 shows a typical Poincaré plot of magnetic field lines in a (θ,r) plane. Periodic fixed points of two kinds appear. The elliptic ones, which are at the centers of the islands, are stable. The hyperbolic ones, i.e., the intersection points of the

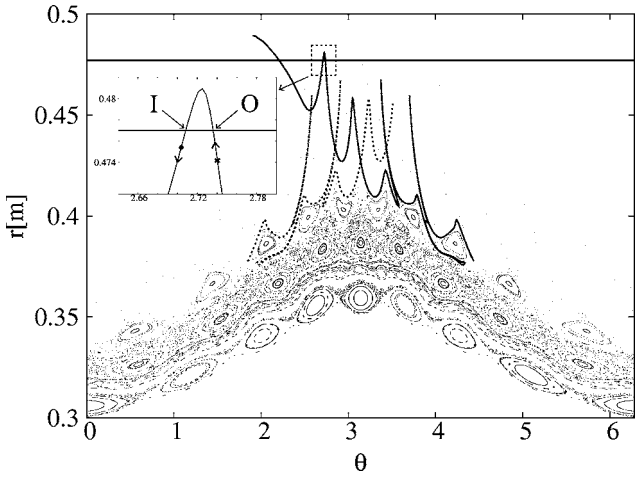

FIG. 3. Poincaré plot of magnetic field lines for q_a=3.23. Stable (dashed line) and unstable (solid line) manifolds of one hyperbolic fixed point of the period-9 island chain are depicted. The inlet shows the manifold close to the wall, leading to the inner (I) and outer (O) branches, respectively.

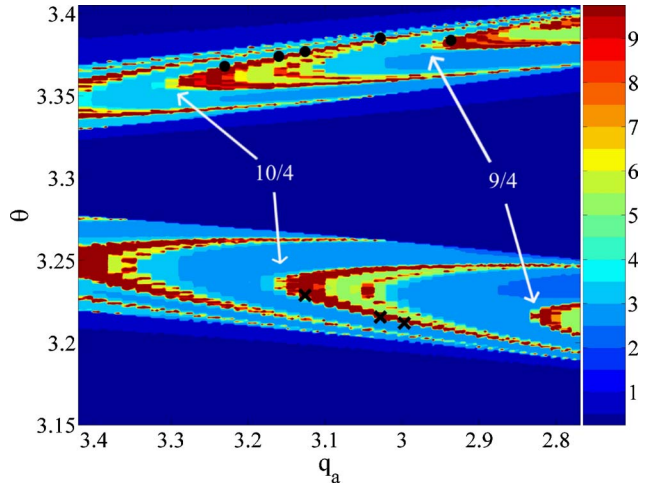

FIG. 4. (Color online) Detailed analysis of three strike zones of Fig. 2. The beginning of a new strike zone is marked by white arrows. The rotational numbers of the corresponding resonances are given. Strike points of several stable (crosses) and unstable (dots) manifolds are shown.

unperturbed separatrices, are located between the islands. They are unstable. A field line close to the hyperbolic point follows a hyperbolic orbit away from the fixed point. The hyperbolic points and their unstable manifolds are the source of chaos and anomalous transport.[8]

C. Calculation of stable and unstable manifolds

A periodic fixed point with period n is defined through

$$\psi = M_{\psi}^{n}(\psi, \vartheta), \quad \vartheta = M_{\vartheta}^{n}(\psi, \vartheta) \bmod 2\pi \tag{8}$$

with M_{ψ}^{n} and M_{ϑ}^{n} being the n-times iterations of the map with respect to ψ and ϑ, respectively. Hyperbolic points can be determined numerically using a minimization method.[44,45] The procedure converges very fast and leads to both types of fixed points up to the desired accuracy. The fixed point being found depends on the choice of the first starting point. The best way to find fixed points in a certain area is to use a grid of starting points.

Coming back to Fig. 3, three main resonances can be observed: the 10/4 island chain, which is the last resonance in front of the wall (at the transition to the laminar zone), the 9/4 island chain (embedded in the chaotic sea), and the 8/4 resonance (beneath the last closed flux surface). Stable and unstable manifolds of hyperbolic points of the period-10 island chain are plotted. The manifolds behave strongly oscillatory, close to a hyperbolic point.[8] The stable and unstable manifolds intersect infinite times, while the area enclosed by the intersections is preserved. Field lines iterate from one area to another.[9] The manifolds shown in Fig. 3 oscillate around the islands, leave the area around the last island chain (10/4 resonance) with large loops, and hit the wall. The wall (target) is the straight line at the top of the figure. Manifolds of different island chains interact, leading to a rapid field line transport from the inside of the torus to the outside.[9]

IV. MOTION OF HOT PARTICLES TOWARD THE WALL

A. Traces of manifolds at the wall

Strike points of the stable and unstable manifolds with the wall lie in the red-colored areas of Fig. 2. Field lines following the manifolds deeply penetrate into the plasma, opening a channel for heat transport from the interior to the strike points. Both the unstable and stable manifolds are important. The plasma particles are either copassing or counterpassing,[31,32] which means that they are either moving in the direction of the field lines (following the unstable manifold), or against (following the stable manifold).

A magnetic field line escaping from the plasma will pierce the plane at discrete points close to the unstable manifold of a hyperbolic fixed point of the last resonant island chain. When continuing, e.g., the unstable manifold, beyond the first wall contact, an additional part of the manifold appears which turns around in a loop and reenters the system (until it leaves the system again). Additional intersections of the manifold with the wall occur. This is sketched in the inlet of Fig. 3 for an unstable manifold. The unstable manifold describes the unstable direction of the intersection points of field lines in the Poincaré section. Not all field lines that follow the unstable manifold leave the system at the first wall contact of the manifold. Some skip the first loop and leave the system close to the next outgoing wall intersection of the manifold. One field line (marked in the inlet by a dot) may have skipped the first external loop. Another field line (marked in the inlet by a cross) intersects with the Poincaré section on the first outgoing part of the unstable manifold very close to the wall. It leaves the system near the first wall contact of the manifold. Both field lines have large connection lengths. However, hot particles following the field lines strike the wall only at the outgoing parts of the manifold. Translating the findings of Fig. 3 into Fig. 2, the inner (I) and

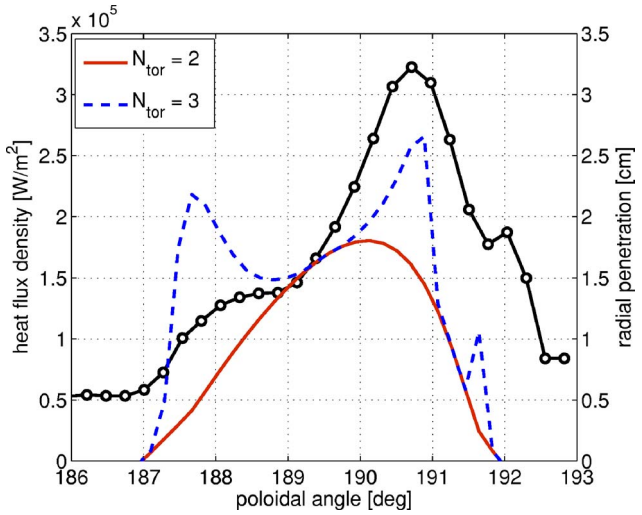

FIG. 5. (Color online) Upper-part strike zone of Fig. 1 (also corresponding to Fig. 2 at a slightly different toroidal position) at $t=2460$ ms for $q_a=2.7$. The black curve (solid line with circles) shows at the left ordinate the heat flux density as a function of the poloidal angle. The red (solid) and blue (broken) curves represent the radial penetration (right ordinate) of the magnetic field lines traced from the target surface, after two and three toroidal revolutions, respectively.

outer (O) branches of the boomerang-shaped strike zones are related to the incoming (I) and outgoing (O) parts of the manifolds, respectively.

The upper part of the two-stripe structure shown in Fig. 2 is created by the unstable manifolds, while the lower one originates from the stable manifolds. This prediction is confirmed by experimental observations[38] when the direction of particle motion is analyzed. The first strike points (O) of stable and unstable manifolds are marked in Fig. 4 by crosses and dots, respectively. The inner branches of the strike zones of Fig. 2 correspond to magnetic field lines with large connection lengths, but no attractive long distance particle motion toward the wall. Short distance motion may occur in the direction opposite to the magnetic field line. However, then the particles are cold and do not deposit a significant amount of heat.

When decreasing the edge safety factor, the resonances are shifted toward the wall and are destroyed. Each strike zone is directly related to the last resonance at the edge of the ergodic zone. At a certain point when (with decreasing q_a values) an island chain is destroyed, the next resonance becomes dominant, which results in a new strike zone. Previously dominant resonances do not disappear completely, explaining the overlapping of the strike zones. According to Fig. 4, the strike zones related to the same resonance appear at smaller values of q_a the closer the parts of the stripes are to the symmetry axis $\theta=\pi$. This effect is caused by the Shafranov shift of the magnetic flux surfaces inside the plasma.

B. Relation with the MASTOC criterion

Finally, we quantify the heat pattern selection criterion and relate it to the MASTOC criterion. The latter states that the power deposition is proportional to the radial penetration of the laminar zone flux tubes over a finite parallel length.[33] Figure 5 shows the heat flux profile (black curve, left ordinate) as a function of the poloidal angle for the discharge presented in Fig. 1 at $t=2460$ ms for $q_a=2.7$. The data correspond to the strike zone in the upper right corner of Fig. 1. There are two branches with enhanced heat deposition, the one with high heat flux density (outer branch) at $\theta\approx 191°$, and the area at $\theta\approx 188°$ with low heat flux density (inner branch). The plot is overlaid with calculated radial penetration depths of the magnetic field lines leaving the target surface (right ordinate). The radial penetration is in plasma coordinates relative to the plasma boundary after two (red curve) and three (blue curve) toroidal turns N_{tor}, respectively. For $N_{\mathrm{tor}}=2$, the field lines at $\theta\approx 190°$ penetrate much deeper into the plasma volume (penetration depth $\geqslant 1.7$ cm with a temperature difference of $kT_e\approx 60$–80 eV) than those at $\theta\approx 188°$ with a penetration depth of $\leqslant 0.5$ cm. The MASTOC criterion would predict from here the preferential heat deposition at $\theta\approx 190°$. For $N_{\mathrm{tor}}=3$, the penetration depths of both bundles of magnetic field lines become similar. We have maxima at $\theta\approx 191°$ (outer branch) and $\theta\approx 188°$ (inner branch). However, the field line dynamics is fundamentally different. Field lines targeting at $\theta\approx 188°$ mainly move in the outer region and only briefly touch the inner hot plasma region. On the other hand, the field line motion to $\theta\approx 191°$ consists of a longer wandering in the inner hot plasma region (at large penetration depth) and a relatively rapid movement through the cold area. This is another view of the magnetic field line behavior, however with the same result as following from the analysis of stable and unstable manifolds of the last island chain.

V. SUMMARY

We have analyzed typical heat flow patterns which appear due to ergodization of a plasma edge. Necessary for significant heat loads are sufficiently large connection lengths to shortcut the (inner) hot plasma with the wall. Large connection lengths of the magnetic field lines are not sufficient. Particle motion should also converge toward the magnetic field lines, which rapidly penetrate from the inside to the outside. Those magnetic field lines, which satisfy the attractive requirement, are close to the unstable (for comoving particles) and stable (for countermoving particles) manifolds of the hyperbolic fixed points of the last intact island chain. The direction of particle motion should be toward the wall. The experimental results from TEXTOR-DED fully support this selection criterion. It is important to note that the criterion is quantitatively equivalent to the so-called MASTOC criterion.[33] The simple nature of the pattern selection principle predestinates it for many future applications, e.g., to diagnose properties of a perturbed volume.

ACKNOWLEDGMENTS

Discussions with Ulrich Samm and Robert Wolf are gratefully acknowledged.

The work was performed under the auspices of the SFB 591.

APPENDIX: EQUILIBRIUM PLASMA CONFIGURATION AND MAGNETIC PERTURBATIONS

For the analysis in the main part of the paper we used as the magnetic field configuration the TEXTOR-DED.[11] The magnetic field is described by the magnetic vector potential **A**. The vector potential includes the magnetic equilibrium field as well as the perturbation field.

We model the plasma with nested, circular magnetic surfaces with the outward (Shafranov) shift of magnetic surfaces due to effects of the plasma pressure and electric current. Let a and $R_0(a)$ be the plasma minor radius and the major radius of the center of the last magnetic surface, respectively. Then, the shift $\Delta(\rho)$ of the major radius of the center of the magnetic surface of radius ρ form $R_0(a)$ is given by[46]

$$\Delta(\rho) = [R_0^2(a) + (\Lambda+1)(a^2-\rho^2)]^{1/2} - R_0(a), \tag{A1}$$

where $\Lambda = \beta_{\mathrm{pol}} + l_i/2 - 1$, $\beta_{\mathrm{pol}} = 8\pi\langle p\rangle/\langle B_\theta\rangle^2$ is the ratio of the plasma pressure $\langle p\rangle$ to the magnetic pressure $\langle B_\theta\rangle^2/8\pi$ of the poloidal field B_θ; l_i is the internal inductance. Furthermore, we consider only the low β and large aspect ratio tokamak plasma.

In the cylindrical coordinate system (R,φ,Z) the magnetic field of the equilibrium plasma can be presented by the vector potential,

$$\mathbf{A} = (0, A_\varphi(r,\theta), A_z(r,\theta)),$$

$$A_\varphi(r,\theta) = \frac{B_0 R_0^2}{R}\int \frac{d\psi}{q(\rho(\psi))},$$

$$A_z(r,\theta) = -B_0 R_0 \ln(R/R_0), \tag{A2}$$

where r,θ are toroidal coordinates related to (R,Z): $R=R_0+r\cos\theta$, $Z=r\sin\theta$, $A_z(r,\theta)$ corresponds to the toroidal field $B_\varphi = B_0R_0/R$, and $A_\varphi(r\theta)$ corresponds to the poloidal field,

$$B_\theta(r,\theta) = \frac{B_0}{qR}\frac{d\psi}{d\rho}\frac{1}{1+\Delta'(\rho)\cos\bar{\theta}}, \tag{A3}$$

where $\bar{\theta} = \sin^{-1}(r\sin\theta/\rho)$. One should note that the Hamiltonian function of field lines is expressed through the toroidal component of the vector potential via $H = -RA_\varphi/B_0R_0^2$.

The safety factor $q(\rho)$ is a function of the radius ρ of a magnetic surface which is related to the normalized toroidal magnetic flux ψ,

$$\psi = \frac{R_0(\rho)}{R_0(a)}\left[1 - \left(1 - \frac{\rho^2}{R_0^2(\rho)}\right)^{1/2}\right] \approx \frac{\rho^2}{2R_0^2(a)}. \tag{A4}$$

The relation between ρ and the toroidal coordinates (r,θ) is

$$\rho = \sqrt{(r\cos\theta - \Delta(\rho))^2 + r^2\sin^2\theta}.$$

In a cylindrical plasma one can use the following model for the safety factor (see Ref. 22):

$$q_{\mathrm{cyl}}(\rho) = q_a\frac{\rho^2}{a^2}\left[1 - \left(1 - \frac{\rho^2}{a^2}\right)^{\nu}\right]^{-1}, \quad \text{for } \rho \leqslant a,$$

$$q_{\mathrm{cyl}}(\rho) = q_a\frac{\rho^2}{a^2}, \quad \text{for } \rho > a,$$

$$q_a = \frac{2\pi B_0 R_0 a^2}{\mu_0 I_p}, \tag{A5}$$

where q_a is the safety factor at the plasma edge a, I_p is the total plasma current, and the exponent is $\nu = q_a/q_0$.

The safety factor given by Eq. (A5) is valid only for the cylindrical plasma column. For large aspect ratios $R/r \gg 1$ the safety factor due to toroidicity can be presented as a series of powers of the inverse aspect ratio $\varepsilon = \rho/R_p(\rho)$ (see Ref. 16),

$$q(\rho) = q_{\mathrm{cyl}}(\rho)\frac{R_0^2}{R_p^2(\rho)}\left(1 + \frac{a_2}{2}\varepsilon^2 + \frac{3a_4}{8}\varepsilon^4 + O(\varepsilon^8)\right), \tag{A6}$$

where $q_{\mathrm{cyl}}(\rho)$ is described by (A5) and the coefficients a_m are given by

$$a_m = (-1)^m\sum_{k=0}^{m}(m-k+1)\Lambda^k. \tag{A7}$$

According to Refs. 11 and 16, the static perturbation magnetic field created by the external TEXTOR-DED coils without the plasma response is mainly determined by its toroidal component of the vector potential $A_\varphi^{(\mathrm{pert})}(r,\theta,\varphi)$. The normalized to $B_0R_0^2/R$ vector potential, i.e., $f_\varphi^{(1)} = B_0R_0^2A_\varphi^{(\mathrm{pert})}/R$, is approximated as

$$f_\varphi^{(1)}(r,\theta,\varphi) = \varepsilon\sum_m f_m(r,\theta)\cos(m\theta - n\varphi + \chi_{mn}), \tag{A8}$$

with the Fourier modes

$$f_m(r,\theta) = -\frac{r_c}{mR_0}g_m\sqrt{1 + \frac{r_c\cos\theta}{R_0}}\left(\frac{r}{r_c}\right)^m, \tag{A9}$$

$$g_m = (-1)^m\frac{\sin[(m - nm_0/4)\theta_c]}{(m - nm_0/4)\pi}. \tag{A10}$$

Here $\varepsilon = B_c/B_0$ stands for the perturbation parameter, $B_c = \mu_0 I_d m_0/(\pi r_c)$ is the characteristic value of the DED magnetic field perturbation, r_c is the minor radius of the DED coils, $\theta_c \approx \pi/5$ is the half angle area of the coils, $m_0 \approx 20$, I_d is the DED current.

The Fourier coefficients $H_{mn}(\psi)$ of the perturbation Hamiltonian (4) are related to the coefficients $f_m(r,\theta)$ through the Fourier integrals

$$H_{mn}(\psi) = \frac{1}{2\pi}\sum_{m'}\int_0^{2\pi} f_{m'}(r,\theta)e^{i(m'\theta(\vartheta) - m\vartheta)}\,d\vartheta, \tag{A11}$$

where the geometrical toroidal angle $\theta(\vartheta)$ is a function of the intrinsic poloidal angle ϑ, which depends on the equilibrium plasma.

The properties of the mode transformation of the spectra of perturbations $f_{m'}(r,\theta)$ in the geometrical space to the $H_{mn}(\psi)$ in intrinsic coordinates have been studied in Refs. 11, 16, and 19.

[1] J. Guckenheimer and P. Holmes, *Nonlinear Oscillations, Dynamical Systems, and Bifurcations of Vector Fields* (Springer, New York, 1983).
[2] F. Casse, M. Lemoine, and G. Pelletier, Phys. Rev. D **65**, 023002 (2001).
[3] A. Shalchi, J. W. Bieber, W. H. Matthaeus, and R. Schlickeiser, Astrophys. J. **642**, 230 (2006).
[4] W. M. Stacey, *Fusion Plasma Physics* (Wiley-VCH, Weinheim, 2005).
[5] E. da Silva, I. Caldas, R. Viana, and M. Sanjuán, Phys. Plasmas **9**, 4917 (2002).
[6] S. S. Abdullaev, T. Eich, and K. H. Finken, Phys. Plasmas **8**, 2739 (2001).
[7] E. Nusse and J. A. Yorke, *Dynamics: Numerical Explorations* (Springer, New York, 1998).
[8] A. Wingen, K. H. Spatschek, and S. Abdullaev, Contrib. Plasma Phys. **45**, 500 (2005).
[9] T. E. Evans, R. K. Roeder, J. A. Carter, and B. I. Rapoport, Contrib. Plasma Phys. **44**, 235 (2004).
[10] T. E. Evans, R. K. Roeder, J. A. Carter, B. I. Rapoport, M. E. Fenstermacher, and C. J. Lasnier, J. Phys.: Conf. Ser. **7**, 174 (2005).
[11] K. H. Finken, S. S. Abdullaev, M. Jakubowski, M. Lehnen, A. Nicolai, and K. H. Spatschek, "The structure of magnetic field in the TEXTOR-DED," in *Energy Technology* (Forschungszentrum Jülich, Jülich, Germany, 2005), Vol. 45 (www.fz-juelich.de/zb/datapool/page/439/00312_Finken.pdf).
[12] R. Balescu, *Statistical Dynamics: Matter out of Equilibrium* (Imperial College, London, 1977).
[13] R. Balescu, M. Vlad, and F. Spineanu, Phys. Rev. E **58**, 951 (1998).
[14] R. Balescu, Phys. Rev. E **58**, 3781 (1998).
[15] S. S. Abdullaev, K. H. Finken, A. Kaleck, and K. H. Spatschek, Phys. Plasmas **5**, 196 (1998).
[16] S. S. Abdullaev, K. H. Finken, and K. H. Spatschek, Phys. Plasmas **6**, 153 (1999).
[17] K. H. Finken, S. S. Abdullaev, A. Kaleck, and G. H. Wolf, Nucl. Fusion **39**, 637 (1999).
[18] S. S. Abdullaev, Nucl. Fusion **44**, 12 (2004).
[19] S. S. Abdullaev, *Construction of Mappings for Hamiltonian Systems and Their Applications* (Springer, Berlin, 2006).
[20] S. S. Abdullaev, J. Phys. A **32**, 2745 (1999).
[21] S. S. Abdullaev, J. Phys. A **35**, 2811 (2002).
[22] J. Wesson, *Tokamaks*, in International Series of Monographs on Physics, 3rd ed. (Clarendon, Oxford, 2004), Vol. 118.
[23] A. Boozer and R. White, Phys. Rev. Lett. **49**, 786 (1982).
[24] R. B. White and Y. Wu, Plasma Phys. Controlled Fusion **35**, 595 (1993).
[25] H. E. Mynick, Phys. Fluids B **5**, 1471 (1993).
[26] H. E. Mynick, Phys. Fluids B **5**, 2460 (1993).
[27] M. DeRover, N. J. Lopes Cardozo, and A. Montvai, Phys. Plasmas **3**, 4468 (1996).
[28] M. DeRover, N. J. Lopes Cardozo, and A. Montvai, Phys. Plasmas **3**, 4478 (1996).
[29] R. B. White, Phys. Rev. E **58**, 1774 (1998).
[30] M. DeRover, A. M. Schilham, A. Montvai, and N. J. Lopes Cardozo, Phys. Plasmas **6**, 2443 (1999).
[31] S. S. Abdullaev, A. Wingen, and K. H. Spatschek, Phys. Plasmas **13**, 042509 (2006).
[32] A. Wingen, S. Abdullaev, K. H. Finken, and K. H. Spatschek, Nucl. Fusion **46**, 941 (2006).
[33] F. Nguyen, P. Ghendrih, and A. Grosman, Nucl. Fusion **37**, 743 (1997).
[34] T. E. Evans, R. A. Moyer, K. H. Burrell, M. E. Fenstermacher, I. Joseph, A. W. Leonard, T. H. Osborne, G. D. Porter, M. J. Schaffer, P. Snyder *et al.*, Nat. Phys. **2**, 419 (2006).
[35] P. Ghendrih, A. Grossman, and H. Capes, Plasma Phys. Controlled Fusion **38**, 1653 (1996).
[36] R. Balescu, *Aspects of Anomalous Transport in Plasmas* (IOP, Bristol, 2005).
[37] T. Evans, R. Moyer, P. Thomas, J. Watkins, T. Osborne, J. Boedo, E. Doyle, M. Fenstermacher, K. Finken, R. Groebner *et al.*, Phys. Rev. Lett. **92**, 235003 (2004).
[38] M. Jakubowski, S. Abdullaev, K. Finken, and the TEXTOR team, Nucl. Fusion **44**, 1 (2004).
[39] M. W. Jakubowski, S. S. Abdullaev, K. H. Finken, M. Lehnen, and the TEXTOR team, J. Nucl. Mater. **337–339**, 176 (2005).
[40] M. Jakubowski, O. Schmitz, S. Abdullaev, S. Brezinsek, K. Finken, A. Krämer-Flecken, M. Lehnen, U. Samm, K. Spatschek, B. Unterberg *et al.*, Phys. Rev. Lett. **96**, 035004 (2006).
[41] A. H. Boozer, Phys. Fluids **26**, 1288 (1983).
[42] R. Balescu, *Transport Processes in Plasmas: 2. Neoclassical Transport Theory* (North-Holland, Amsterdam, 1988).
[43] A. H. Boozer, in *Encyclopedia of Physical Science and Technology* (Academic, New York, 1992), Vol. 13.
[44] J. H. Misguich, J.-D. Reuss, D. Constantinescu, G. Steinbrecher, M. Vlad, F. Spineanu, B. Weyssow, and R. Balescu, Ann. Phys. (Paris) **286**, 87 (2003).
[45] G. Steinbrecher, J.-D. Reuss, and J. H. Misguich, EURATOM-CEA, Cadarache, St. Paul-lez-Durance, France, Report No. EUR-CEA-FC-1719, 2001.
[46] F. Nguyen, P. Ghendrih, and A. Samain, EURATOM-CEA, Cadarache, St. Paul-lez-Durance, France, Report No. DFRC/CAD EUR-CEA-FC-1539, 1995.